Visible Light Sensitization of TiO_2 Surfaces with Alq3 Complexes

Luis G. C. Rego,*,† Robson da Silva,‡ José A. Freire,§ Robert C. Snoeberger,|| and Victor S. Batista*,||

Department of Physics, Universidade Federal de Santa Catarina, Florianópolis, SC, 88040-900, Brazil, Department of Chemistry, Universidade Federal de Santa Catarina, Florianópolis, SC, 88040-900, Brazil, Department of Physics, Universidade Federal do Paraná, Curitiba, PR, 81531-990, Brazil, and Department of Chemistry, Yale University, P.O. Box, 208107, New Haven, Connecticut 06520-8107

Received: October 1, 2009; Revised Manuscript Received: November 5, 2009

We combine ab initio DFT molecular dynamics simulations and quantum dynamics propagation of transient electronic excitations to investigate visible light sensitization of TiO_2-anatase surfaces by covalent attachment of derivatized aluminum tris-(8-hydroxyquinoline) (Alq3) complexes. Hydroxylated arylquinoline and benzoquinoline ligands are introduced as robust anchoring groups to form Alq3/TiO_2 molecular assemblies. We show that photoexcitation of the resulting surface complexes with visible light triggers ultrafast interfacial electron injection into the TiO_2 host substrate. Furthermore, we show that derivatization of the Alq3/TiO_2 surface complexes with oligothiophenes should hinder electron−hole pair recombination after photoinduced interfacial electron transfer. These findings are particularly relevant to the development of molecular based photo-optic devices based on the general class of metaloquinolate complexes Mq3, with q = 8-hydroxyquinoline and M = Al, Zn, Ga, and In, which have already attracted significant interest in the development of new technologies.

1. Introduction

The discovery of organic light emitting diodes (OLEDs) based on aluminum tris-(8-hydroxyquinoline) (Alq3) represented a significant technological breakthrough[1] after decades of research in organic optical media for electroluminescent (EL) devices.[2−5] Highly efficient, long-lasting and low-voltage devices were based on Alq3 thin-films that played the double role of fluorescent material and electron transport layer. Several variations of the original Alq3-OLED design (see Figure 1) were subsequently proposed, including devices with additional transport layers that improved the mobility of electrons and holes,[6,7] as well as designs with doped Alq3 layers to increase the fluorescence quantum efficiency and tune the color of the luminescent light.[6] Other combinations of interfaces improved the overall stability and lifetime of the resulting devices.[8,9] With all these developments, Alq3 has become a prototypical optical medium currently available in several commercial OLEDs. However, the capabilities of Alq3 complexes as a visible-light sensitizer for applications to photo-optic devices have yet to be investigated. In this paper, we build upon our earlier studies,[10−14] and we combine ab initio DFT molecular dynamics simulations and quantum dynamics propagation of transient electronic excitations to investigate the sensitization of TiO_2-anatase by covalent attachment of derivatized Alq3 complexes.

Previous studies of Alq3 in solar cells have been limited to the analysis of Alq3 thin-films as electron transport layers,[15] or buffer films to prevent diffusion of cathode atoms (generally Au and Al) into the underlying optical layer.[16] In addition, Alq3 has been studied at interfaces with oxides[17] and metals,[18−20] but studies of Alq3/TiO_2 interfaces have yet to be reported. Here,

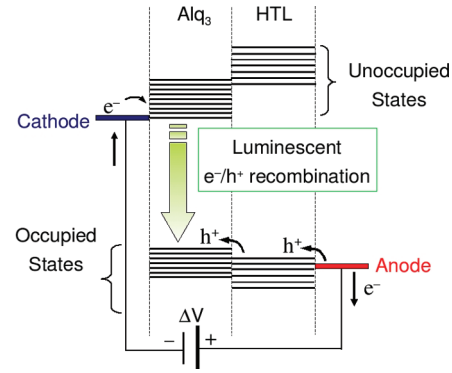

Figure 1. Schematic energy diagram of a double layer Alq3-OLED, including the luminescence due to e^-/h^+ recombination, the metallic cathode, the Alq3 film, the hole-transport layer (HTL), and the transparent anode (generally an indium−tin−oxide film).

we investigate Alq3 complexes anchored to TiO_2-anatase surfaces by using hydroxylated arylquinoline and benzoquinoline ligands as a new class of linkers that form robust Alq3/TiO_2 molecular assemblies. We show that these linkers shift the photoabsorption threshold of Alq3 (ca. 3.2 eV) into the visible region when covalently bound to TiO_2 and explore whether the derivatization of the Alq3/TiO_2 surface complexes with oligothiophenes should hinder electron−hole pair recombination after photoinduced interfacial electron transfer in photovoltaic devices. The reported studies are expected to stimulate experimental work since they are particularly valuable for the development of photo-optic devices based on inexpensive metal (Al) complexes. An example is the photovoltaic cell depicted in Figure 2. The materials investigated also offer an opportunity to explore interfacial photoconversion mechanisms in Al complexes (Alq3) that have already attracted significant interest in the development of organic light-emitting devices.[1]

* To whom correspondence should be addressed.
† Department of Physics, Universidade Federal de Santa Catarina.
‡ Department of Chemistry, Universidade Federal de Santa Catarina.
§ Universidade Federal do Paraná.
|| Yale University.

10.1021/jp9094479
Published on Web 12/08/2009

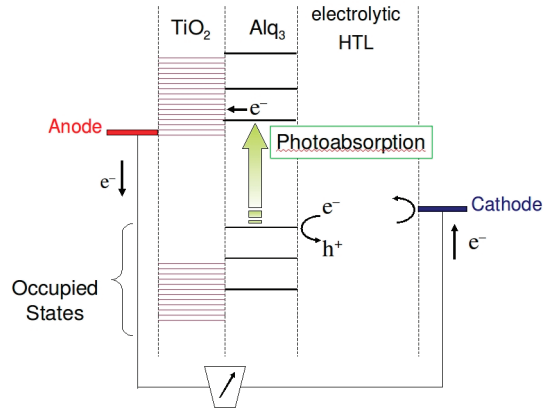

Figure 2. Schematic energy diagram of an Alq3 dye-sensitized solar cell, including the anode, the porous TiO_2 thin-film, the discrete energy levels of Alq3, the electrolytic HTL, and the cathode. The arrows indicate the photoexcitation of Alq3, followed by electron injection into TiO_2.

Dye-sensitized solar cells have received widespread attention as they offer the possibility of low cost and high solar-to-electricity conversion efficiency. Innumerable sensitizers have been tested experimentally, including simple dyes, polymers, and supramolecular systems,[21−23] These trials, however, have failed to improve the overall efficiency of the original Grätzel cell.[24] From the theoretical point of view, the description of the interfacial electron transfer (IET) has improved with the development of new computational methods,[26−28] but a comprehensive description of all the charge transfer processes that are responsible for the operation of a dye sensitized solar cell, including the solvent and the redox pairs as well as recombination, dye-regeneration, and back-electron transfer effects, is still not available.

Figure 2 shows a schematic energy diagram of a solar cell based on TiO_2 thin-films sensitized with Alq3 complexes. Note that the operational mode of this photovoltaic device would be reverse relative to the OLED shown in Figure 1. While the OLED produces light by electron−hole pair recombination, the solar cell shown in Figure 2 absorbs light to induce electron−hole pair separation by interfacial electron transfer into TiO_2. Therefore, to investigate its feasibility, it is important to analyze the photoabsorption process and the interfacial electron transfer in Alq3/TiO_2 molecular assemblies.

We study fully atomistic models of TiO_2 nanoparticles functionalized with Alq3, where one of the quinoline ligands is derivatized to function as a Lewis base anchoring group. We analyze hydroxylated arylquinoline and benzoquinoline moieties as well as quinoline ligands derivatized with oligothiophenes. As in previous studies,[10−14] our quantum dynamics simulations analyze the ensuing interfacial electron transfer into the conduction band of the TiO_2 host substrate after photoexcitation of the surface complexes covalently attached to the semiconductor surface.

The paper is organized as follows. The structural models and the computational methods are described in Section 2. The photophysical properties of Alq3 complexes are discussed in Section 3. Then, the sensitization of TiO_2-anatase to visible light by functionalization with Alq3 is analyzed in Section 4. The electronic states of Alq3-dithiophene/TiO_2 assemblies is analyzed in Section 5. Finally, our concluding remarks are presented in Section 6.

2. Models and Methods

2.1. Structural Models. Minimum energy structures of Alq3 and Alq3-derivatives in their ground electronic state were obtained at the DFT level by using the Becke three-parameter Lee−Yang−Parr (B3LYP) hybrid functional[29] and the 6-31G(d) basis set as implemented in Gaussian 03.[30] Minimum energy structures in the first singlet excited state (S_1) were obtained by structural optimization at the ab initio configuration interaction singles (CIS) level in the frozen-core approximation. The excited state electronic structures and the optical transitions were subsequently computed at the time-dependent density functional theory (TDDFT) level, using the same hybrid density functional and basis set (B3LYP/6-31G(d)).

The minimum energy structures and molecular dynamics (MD) simulations of semiconductor supercells modeling TiO_2-anatase surfaces sensitized with derivatized Alq3 complexes were obtained at the DFT level, using periodic boundary conditions as implemented in the Vienna ab initio Simulation Package.[31−33] VASP is a highly efficient simulation package for DFT studies of extended systems. Calculations are based on plane-wave expansions of the Kohn−Sham orbitals. We applied the generalized gradient approximation (GGA) together with the Perdew−Wang (PW91) exchange-correlation functional and ultrasoft pseudopotentials for describing the electron-ion interactions. This level of theory predicted minimum energy configurations for the isolated Alq3 and derivatized Alq3 complexes in excellent agreement with those obtained at the DFT/B3LYP level with Gaussian 03. All initial-guess configurations necessary for DFT geometry optimization were generated by simulated annealing at the AM1 semiempirical level of theory, as implemented by the program pdynamo.[34]

2.2. Electronic Structure Calculations. The density of states, the photoabsorption spectra, and the simulations of quantum dynamics in Alq2(L)/TiO_2 supercells were based on a tight-binding model Hamiltonian gained from the semiempirical Extended-Hückel (EH) method. The EH tight-binding Hamiltonian has been extensively applied in studies of molecular and periodic systems,[35−37] including several studies of sensitized TiO_2 surfaces.[10−14] The method requires a small number of transferable parameters (1−9 parameters per atom),[38] providing an excellent cost-benefit option for the description of quantum dynamic processes in very large systems.

We compute the EH Hamiltonian in the basis of Slater-type orbitals (STO) for the radial part of the atomic orbital wave functions.[39] The basis set includes the 3d, 4s, and 4p atomic orbitals of Ti^{4+} ions, the 3s and 3p orbitals of Al^{3+} ions, the 2s and 2p orbitals of O^{2-} ions, C and N atoms, and the 1s orbital of H atoms. Having defined the atomic orbitals $\{|\phi_i\rangle\}$, the overlap and the off-diagonal Hamiltonian matrix elements can be computed, respectively, as $S_{ij} = \langle\phi_i|\phi_j\rangle$ and $H_{ij} = K'S_{ij}(H_{ii} + H_{jj})/2$. We implement the more accurate Wolfsberg−Helmholz formula,[40] giving $K' = K + \Delta^2 + \Delta^4(1 - K)$, where K is the original Wolfsberg−Helmholz empirical parameter and $\Delta = (H_{ii} - H_{jj})/(H_{ii} + H_{jj})$. We verified that the value $K = 1.75$ provides a good description of the TiO_2 semiconductor while $K = 2.0$ produces energy levels for Alq3 and Alq2(L) moieties that are in close agreement with the experimental data. No energy shifts or further corrections were necessary for either the occupied or unoccupied states of the EH calculations beyond the original parametrization.[41] In addition, in the Alq3/TiO2 surface the energy difference between the adsorbate excited state and the edge of the conduction band is large compared to the exciton binding energy.

2.3. Quantum Dynamics. The simulations of interfacial electron transfer dynamics are based on the mixed quantum-classical method previously implemented in studies of electron injection in sensitized TiO_2 surfaces.[10−14] To avoid unphysical recurrences due to periodic boundary conditions, our simulations of the electronic quantum dynamics are performed in 3 × 3 extended nanostructures constructed by the juxtaposition of nine supercell units, described in Figures 4 and 5. The resulting mixed quantum-classical simulations of electron injection in sensitized TiO_2 surfaces are in very good agreement with experimental data[42,43] and with the description of dynamics provided by other approximate computational approaches.[44−47]

The initial state $|\Psi_0\rangle$ of the photoexcited electron is assumed to be localized in the adsorbate molecule as it would result from a $\pi^* \leftarrow \pi$ excitation in a hydroxyquinoline ligand of the metal complex, or a metal-to-ligand transition. Since that initial state is not an eigenstate of the complete supercell Hamiltonian $\hat{H}$, it evolves in time as described by the time-dependent wave function

$$|\Phi(t)\rangle = \sum_{i,\alpha} B_{i\alpha}(t)|i\alpha\rangle \tag{1}$$

Here, we expanded $|\Phi(t)\rangle$ as a linear combination of atomic orbitals, with $|i\alpha\rangle$ designating the atomic orbital α belonging to atom i. The expansion coefficients $B_{i\alpha}(t)$, introduced by eq 1, are computed as follows

$$B_{i\alpha}(t) = \sum_{q} \mathbf{Q}^{q}_{i,\alpha} C_q \exp\left(-\frac{i}{\hbar} E_q t\right) \tag{2}$$

after solving the generalized eigenvalue equation

$$H\mathbf{Q}^q = E_q S\mathbf{Q}^q \tag{3}$$

Here, H is the EH matrix and S is the overlap matrix in the atomic orbital basis. The coefficients C_q, introduced by eq 2, are defined by the expansion of the initial state in the orthonormal basis set of eigenvectors $|q\rangle$

$$|\Phi(0)\rangle = \sum_{q} C_q |q\rangle \tag{4}$$

The coefficients $\mathbf{Q}^q_{i,\alpha}$, introduced by eq 2, are defined according to the expansion of the eigenvectors $|q\rangle$ as a linear combination of atomic orbitals

$$|q\rangle = \sum_{i,\alpha} \mathbf{Q}^q_{i\alpha} |i\alpha\rangle \tag{5}$$

Having propagated the time-dependent wave function, $|\Phi(t)\rangle$, we compute the time-dependent electronic population of the adsorbate molecule as the projection of $|\Phi(t)\rangle$ into the atomic orbitals of the molecular adsorbate, as follows

$$P(t) = \left| \sum_{i,\alpha}^{\mathrm{MOL}} \sum_{j,\beta} B^*_{i,\alpha}(t) B_{j,\beta}(t) S^{i,j}_{\alpha\beta} \right| \tag{6}$$

Here, $S^{i,j}_{\alpha\beta} = \langle i\alpha|j\beta\rangle$, where the indices α and β label specific orbitals in atoms i and j, respectively. Note that the sum over j includes all of the atoms in the nanostructure, whereas the sum over i includes only atoms in the initially excited molecular adsorbate.

The EH molecular orbital theory is also applied in our simulations of photoabsorption spectra to obtain the intensities of electronic dipole induced transitions for the Alq2(L)/TiO_2 supercells. The oscillator strength (f) of the one electron transition $\Psi_q \leftarrow \Psi_p$ is obtained as follows[39,48]

$$f_{pq} = \frac{8\pi^2 \bar{\nu} c m_e}{3he^2} \left| \vec{\mu}_{pq} \right|^2 \tag{7}$$

where $\vec{\mu}_{pq} = \langle \Psi_q | e\vec{r} | \Psi_p \rangle$ is the electronic transition dipole moment between molecular orbitals Ψ_q and Ψ_p, $\bar{\nu}$ is the wavenumber of the transition, and m_e is the electron mass. The transition dipole moments are fully computed on the STO basis by using recurrent integrals.[49] The contribution of direct charge transfer excitations to the absorption spectrum in dye sensitized semiconductors, based on a time-dependent formulation, has also been investigated by May and co-workers.[50]

3. Photophysics of Alq_3

The structural, optical, and transport properties of the Alq3 molecule and several of its derivatized complexes have been intensively investigated, particularly after the seminal paper of Tang and Van Slyke.[1] In this section, we outline its main photophysical properties and compare literature results with our own calculations. Figure 3 shows a scheme of the meridian (*mer*) isomer of the Alq3 molecule. We restricted our study to the *mer*-Alq3 isomer since the facial (*fac*) isomer, obtained by rotating one of the hydroxyquinoline rings, was found to be less stable.[51,52]

The optical properties of Alq3 (i.e., absorption and luminescence) are common to the general class of fluorescent metal-chelate complexes Mq3, typically with q = 8-hydroxyquinoline and M = Al, Zn, Ga and In,[7,53] since the frontier orbitals of these complexes are strongly localized in the quinoline rings with only minor contributions from the metal centers.[19,52,54] Our analysis supports the close similarity between the frontier orbitals of the isolated 8-hydroxyquinoline ligand and those of Alq3. Because of the localized nature of the orbitals involved, the lowest energy transitions correspond to $\pi^* \leftarrow \pi$ excitations in the quinolate rings with partial charge transfer from the phenoxide moiety to the pyridyl ring. These excitations determine the photoabsorption threshold at 390 nm (ca. 3.2 eV) even in solid or solution phases.[55] The high photoabsorption threshold in the UV has so far prevented the application of Alq3 as an active optical component in photovoltaic solar cells, limiting technological applications to OLED devices that exploit the photoluminescence of Alq3 at 514 nm.[7]

Several derivatives of the Alq3 complex have been developed since it became evident that the optical properties of Alq3 could be tuned by adding substituents to the quinolate ligand, changing the energy of the occupied or vacant orbitals.[7,19,58,59] Most of this work on Alq3 derivatives has been focused on modulating the photoluminescence properties of OLEDs. The perturbational influence of a surrounding molecular environment has also been investigated.[7,53,58,60−62] It was found that due to the localized nature of the orbitals involved in the electronic transitions both the photoabsorption and photoluminescence spectra of these compounds are typically quite insensitive to the environment (also manifested by the spectroscopy of Alq3 in the solid

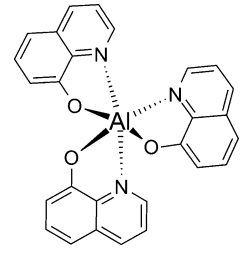

Figure 3. Meridian Alq3 molecule.

TABLE 1: Vertical Excitation Energies (E_n) in eV and Oscillator Strengths (f_n) Obtained at the TD DFT-B3LYP/6-31G(d) Level of Theory for the Electronic State Transitions $S_n \leftarrow S_0$ with $n = 1-4$[a]

	E_1 (f_1)	E_2 (f_2)	E_3 (f_3)	E_4 (f_4)
Alq3 (S_0)	2.76 (0.005)	2.89 (0.067)	2.93 (0.002)	2.95 (0.042)
Alq3 (S_1)	2.29 (0.040)	2.50 (0.002)	2.85 (0.003)	3.01 (0.011)
Alq2(L)	2.52 (0.003)	2.61 (0.034)	2.78 (0.002)	2.85 (0.009)
Complex **2** Ti^{4+} $(H_2O)_2$ $(OH)_2$	2.14 (0.019)	2.21 (0.001)	2.43 (0.018)	2.51 (0.023)

[a] The table includes results for the Alq3 molecule in its S_0 and S_1 minimum energy configurations (rows 1 and 2, respectively). Row 3 refers to the optimized (S_0) Alq2(L) moiety shown in Figure 5a. Complex **2** in row 4 refers to the same Alq2(L) chelating an aqueous Ti^{4+}, also in its S_0 minimum energy configuration.

phase,[7,60,61] in liquid solutions,[53,58,62] and in the gas-phase[55]). Even Alq3-functionalized polymers preserve the fluorescence characteristics of the isolated Alq3 molecule.[58] However, the modulation of the optical properties of Alq3 complexes by functionalization of semiconductor surfaces has yet to be reported and is addressed in the following section.

Table 1 reports time-dependent (TD) DFT-B3LYP/6-31G(d) calculations of vertical excitation energies (E_n) and oscillator strengths (f_n), associated with the first four excited state transitions $S_n \leftarrow S_0$ (with $n = 1-4$). The reported calculations comply with well-known methods adopted in the literature.[52,54] Table 1 shows that the strongest absorption of Alq3 in the ground state occurs at $E_2 = 2.89$ eV (429 nm), while the dominant emission from the S_1 state is centered at 2.29 eV (543 nm). The calculated Stokes-shift of 114 nm is in good agreement with the large experimental Stokes-shift (126 nm) that places the Alq3 broad photoluminescence band centered at 514 nm (2.4 eV).[7] The origin of the Stokes-shift can be traced to the structural relaxation of the excited hydroxyquinoline ligand in the excited state.[64] In addition, the reported results show that functionalization of Alq3 with catechol shifts the dominant absorption from 429 to 475 nm ($E_2 = 2.61$ eV) and, moreover, chelation with Ti^{4+} further shifts the absorption into the visible range to 578−493 nm (2.14−2.51 eV).

The photoabsorption spectrum of Alq3, obtained at the EH level predicts a peak centered at 3.25 eV (381 nm), in close agreement with the HOMO−LUMO gap predicted at the DFT/6-31G(d) level (3.26 eV), and higher energy bands at 4.2 eV (295 nm) and 4.8 eV (258 nm). In addition, the EH method yields a luminescence peak at 2.65 eV (468 nm). These results are in good agreement with experimental data[53,61] and theory.[51,52] The experimental absorption spectrum of Alq3 (in solid, liquid or gas phases) consists of a broad, low-energy band at about 3.22 eV (385 nm), a quasi-flat segment between 3.6 eV (344 nm) and 4.2 eV (295 nm), and a strong narrow-band at 4.77 eV (260 nm).[7,53,55,60,63] The electronic transitions comprising the lowest energy band are $\pi^* \leftarrow \pi$ transitions in the hydroxyquinoline rings, involving partial charge transfer from the phenoxide ring to the pyridyl acceptor. The nature of the second absorption peak, including the quasi-flat segment, are yet to be completely understood. A comprehensive analysis of the optical properties of Alq3 was provided by Choy and Fong.[63] Some studies assigned the two main absorption peaks to the ^1L_a and ^1B_b excited states, whereas the intermediary structure is due to the fast nonradiative relaxation from the ^1B_b to the ^1L_a state and subsequent luminescence.[65]

4. Sensitization of TiO_2 with Alq_3

4.1. Covalent Attachment Schemes. Transition metal complexes can be attached to TiO_2 surfaces by using Lewis bases as molecular linkers.[10−14] In previous work, we have explored several linkers, including catecholate,[10−13] acetylacetonate,[14] and hydroxamate groups. Because of their strong affinity to TiO_2, all of these Lewis base linkers are efficient anchoring groups for attachment of metal complexes to TiO_2.[11,47,66,67] Here, we analyze the covalent attachment of Alq3 to TiO_2 by using catecholate-like linkers.

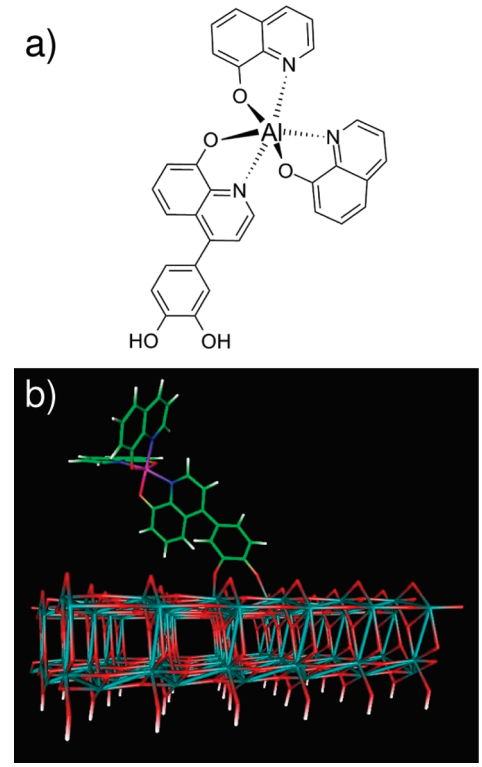

Figure 4. (a) Complex **1**: Alq2(L), with a catechol-substituted 8-hydroxyquinoline ligand; (b) Minimum energy structure of complex **1** adsorbed on the (101) surface of the TiO_2-anatase.

Figure 4a shows the derivatization of one of the 8-hydroxyquinoline ligands with a catechol moiety. The resulting complex **1** binds to the (101) surface of TiO_2 -anatase forming two Ti−O covalent bonds,[10] as shown in Figure 4b. Another derivatization scheme is shown in Figure 5, where one of the 8-hydroxyquinolines in Alq3 is replaced by 6,7,10-trihydroxybenzo(f)quinoline. The resulting complex **2** binds to the (101) surface of TiO_2-anatase analogously to complex **1**, forming two Ti- O covalent bonds as shown in Figure 5b. Because of the similarity with the attachment mode of catechol to TiO_2 -anatase,[68] both complexes **1** and **2** bind strongly to the TiO_2 surface. Our DFT calculations, described in the sequence, predict a dissociative adsorption energy for complex **2** on the (101) anatase surface of −23.3 kcal/mol, in close agreement with calculations of dissociative catechol adsorption reported for small anatase clusters[68] and periodic DFT studies.[69]

The DFT minimum energy structures, shown in Figure 4 and Figure 5, and MD simulations were obtained as described in Section 2.1. The semiconductor was modeled by a supercell of

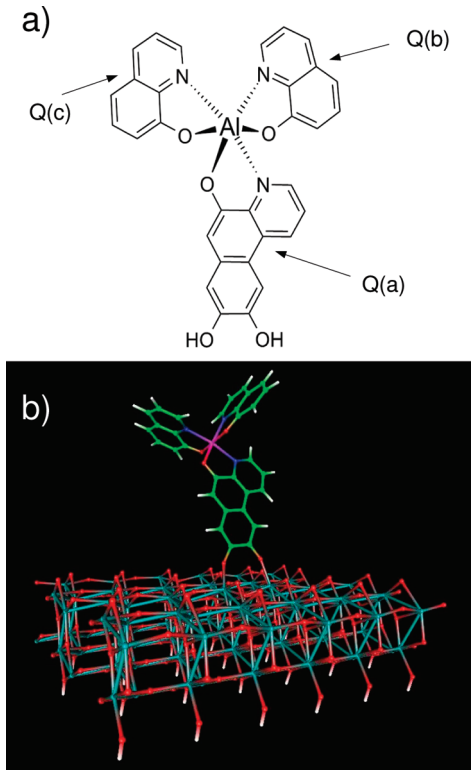

Figure 5. (a) Complex **2**: derivatized Alq3 with one of the hydroxyquinoline ligands replaced by 6,7,10-trihydroxybenzo(f)quinoline. The 8-hydroxyquinoline ligands Q(a), Q(b), and Q(c) are labeled for future reference. (b) Minimum energy structure of complex **2** adsorbed on the (101) surface of the TiO_2-anatase.

96 [TiO_2] units with lateral dimensions of 2.0 nm × 2.4 nm in the directions [101] and [010], respectively. Extended 3 × 3 models constructed by the juxtaposition of nine supercell units were used for quantum dynamics simulations of interfacial electron injection. The dimensions of the unit supercell correspond to typical surface coverage of 1 adsorbate molecule per nm^2 (i.e., 1 μmol m^{-2}).

DFT geometry optimizations as well as DFT molecular dynamics simulations were conducted at the Γ point of the reciprocal space with periodic boundary conditions. The MD simulations were performed at $T = 350$ K to test the stability of the TiO_2-anatase surfaces sensitized with derivatized Alq3 complexes. Dangling bonds in the bottom of the slab were saturated with hydrogen atoms, and a 5.0 nm vacuum spacer was implemented on top of the slab (in the vertical direction [$\bar{1}$01]) to eliminate artificial interactions between the Alq2(L) sensitizer and the bottom of the TiO_2 slab, introduced by the periodic boundary conditions. We expect the formation of stereoisomers to influence the photophysical properties of complex **1**, but not those of complex **2**. Regarding the Alq3 molecule, experimental studies performed by proton-NMR[70] and matrix-isolation IR-spectroscopy (carried at $T = 11$ K)[71] found insufficient evidence for the presence of the facial isomer. In that regard, theoretical calculations predict that the mer-Alq3 isomer is 4 to 8 kcal/mol lower in energy than the fac-Alq3 isomer.[54,71]

4.2. Density of States and Photoabsorption Spectra. Figure 6 shows the electronic density of states (DOS) of the 2 nm supercell of Alq2(L)-TiO_2 shown in Figure 4b (i.e., **1**-TiO_2). In agreement with previous calculations,[10,11] the TiO_2 band gap obtained for this 2 nm model is 3.8 eV (326 nm), slightly larger than the experimental value 3.45 eV (359 nm) reported for larger

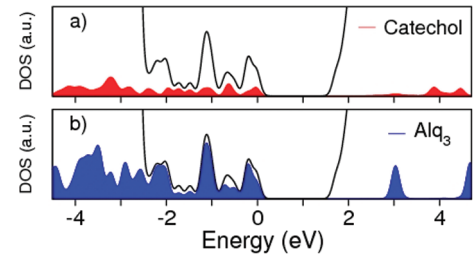

Figure 6. Total electronic density of states (DOS) of **1**-TiO_2 (black line) and projected DOS onto catechol (red) and Alq3 (blue) fragments. For convenience the HOMO is set to zero.

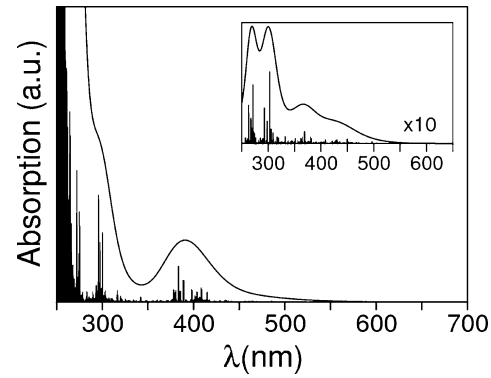

Figure 7. UV−visible absorption spectrum of the **1**-TiO_2 supercell, shown in Figure 4b, calculated at the EH level of theory. Inset: absorption transition lines from the catechol moiety to the unoccupied states of the supercell (complex **1** on TiO_2).

(6 nm) nanoparticles.[72] The projected density of states (PDOS), shown in Figure 6, reveals that the covalent attachment of the Alq2(L) adsorbate introduces electronic states in the TiO_2 band gap. Such states sensitize the TiO_2 nanoparticles to absorption of low energy photons whenever they have optically allowed transitions to the edge of the conduction band.

Figure 7 shows the calculated UV−vis absorption spectrum of the supercell Alq2(L)-TiO_2 (complex **1** on TiO_2) obtained at the EH level. Centered at 3.17 eV (ca. 391 nm) there is a peak, comprised by several transition lines from the HOMO to the LUMO manifold of Alq3 quasi-triplets. Another distinct set of spectral lines occur around 4.2 eV (ca. 295 nm), just before the threshold of the TiO_2 absorption band, which can be ascribed to the Alq3 and catechol moieties, independently. The stronger peaks correspond to electronic transitions within the Alq3 moiety. The weaker ones (inset of Figure 7) give rise to a broad charge-transfer band (350−450 nm) comprised of transitions from the catechol moiety to the unoccupied states of the TiO_2 and a pair of narrower bands centered at 270 nm corresponding to electronic transitions within the catechol moiety. Transitions within the quinoline ligands are not significantly affected by the catechol moiety because of the localized nature of the Alq3 frontier orbitals.The excitation energies of catechol are consistent with the two distinct excitation mechanisms originally revealed by experimental studies.[73] In solution, catechol shows an absorption peak at 275 nm (4.5 eV) and it develops a broad absorption band at 350−450 nm (centered around 390 nm) upon complexation with Ti^{4+} (or when attached to TiO_2 nanoparticles) that can be readily ascribed to electronic state transitions from catechol to the d orbitals of the Ti^{4+} ions.[72−75] These lower energy transitions sensitize TiO_2 to visible-light as predicted for Alq2(L)/TiO_2.

Functionalization of TiO_2 surfaces with complex **2** (shown in Figure 5b) also leads to sensitization of anatase to visible

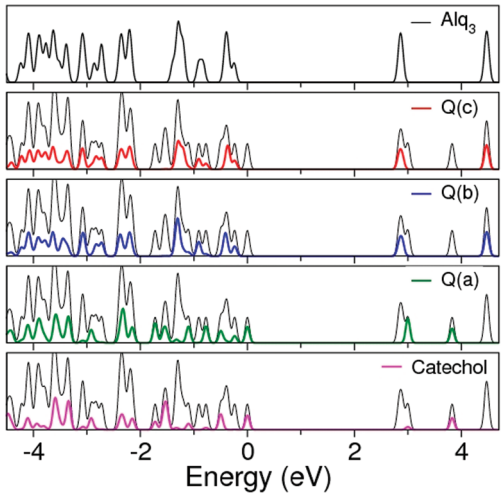

Figure 8. Electronic density-of-states (DOS). Top panel: total DOS of free Alq3. Lower panels: total (black) and projected (red, blue, green) DOS for the Alq2(L) complex, shown Figure 5a. Projections onto the unaltered quinoline rings Q(c) and Q(b) are compared to those onto ring Q(a) and catechol fragment.

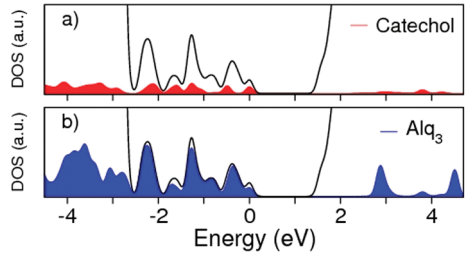

Figure 9. Total electronic density of states (DOS) of the **1**-TiO_2 structure shown in Figure 5b (black line) and PDOS onto catechol (red, a) and Alq3 (blue, b) fragments.

light with an absorption spectrum analogous to Figure 7. Figure 8 and Figure 9 present a detailed analysis of the electronic states responsible for sensitization of TiO_2 to visible light whereas Figure 11 shows the resulting photoabsorption spectrum.

The comparison of the total DOS of free Alq3 (top panel, Figure 8) and the total DOS of complex **2** projected into individual hydroxyquinolines (a−c) and catechol fragments (lower panels, Figure 8) clearly illustrates the net effect of derivatization of Alq3 on the electronic structure of the resulting complex. The replacement of the 8-hydroxyquinoline moiety by 6,7,10-trihydroxybenzo(f)quinoline affects mostly the phenoxide ring and consequently the HOMO state of Q(a). In contrast, the LUMO orbitals are localized in the pyridine rings and therefore remain unaffected by the derivatization of the phenoxy rings.

Figure 10 illustrates the HOMO and LUMO+2 orbitals of complex **2**-TiO_2 in terms of isosurfaces of electronic density. As shown in panel a, the HOMO is delocalized in the phenoxy(f)quinoline moiety, equally shared by both aromatic rings. Further insight about the system can be gained by comparing the Q(a)-catechol ligand with the alizarin dye.[56,57] Like our phenoxy(f)quinoline moiety, the HOMO of free alizarin is a π orbital localized toward the hydroxyl end of the molecule. Ab initio electronic structure calculations[57] performed for the alizarin molecule evince that binding alizarin to Ti causes a redistribution of electron density that reduces the HOMO−LUMO gap and red shifts the molecular spectrum. The same effect occurs in the **2**-TiO_2 system, as reported in Figure 9. We have also performed energy calculations by the TDDFT-B3LYP/6-

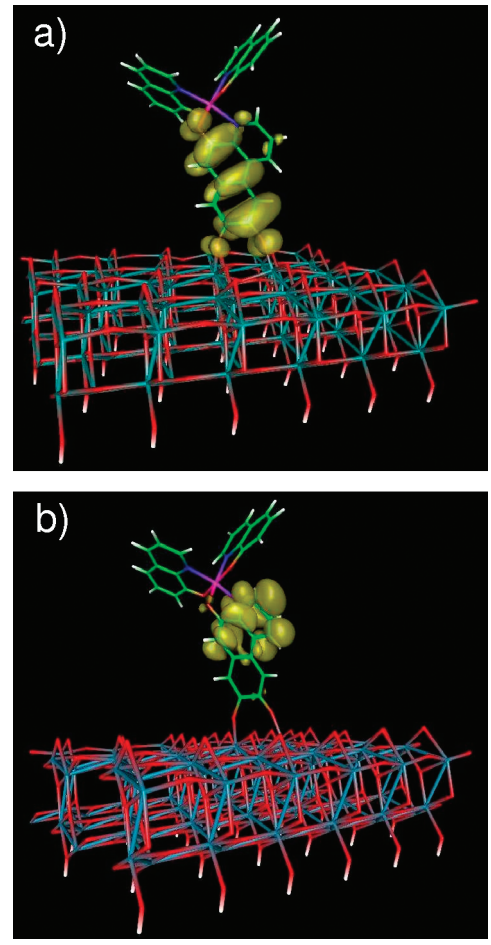

Figure 10. Charge density isosurfaces for the least bound HOMO (a) and the LUMO+2 (b) orbitals of complex **2**-TiO_2.

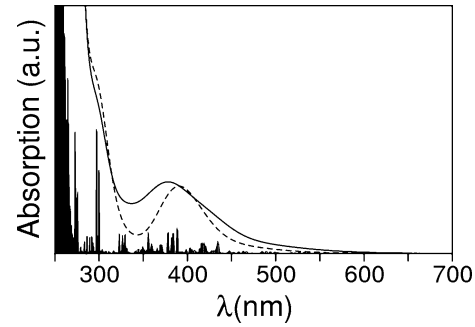

Figure 11. Calculated UV−visible photoabsorption spectrum of the supercell **2**-TiO_2, shown in Figure 5b (solid-line), compared to the absorption spectrum of **1**-TiO_2 (dashed-line).

31G(d) method for complex-**2** chelating an aqueous Ti^{4+}, reported in Table 1. The calculations show a consistent reduction of both the ground-state HOMO−LUMO gap and the excitation energies, in accordance with the PDOS of Figure 9 and the calculated UV−visible photoabsorption spectrum of **2**-TiO_2 shown in Figure 11.

4.3. Ultrafast Electron Injection. Figure 12 shows the calculated time-dependent electronic population $P(t)$ of a photoexcited Alq3 adsorbate in the supercell **1**-TiO_2, shown in Figure 4, after photoexcitation of the complex to the LUMO (red), LUMO+1 (blue), and LUMO+2 (green) states. Figure 12 shows that the electron injection from the LUMO+1 and LUMO+2 of Alq3 involve subpicosecond time-scales. In contrast, the interfacial electron injection from the LUMO is

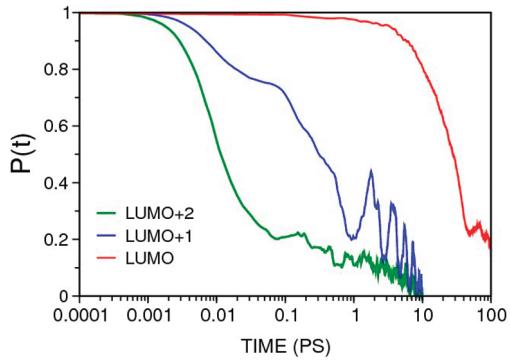

Figure 12. Survival probability curves for electron injection from the LUMO (red), LUMO+1 (blue), and LUMO+2 (green).

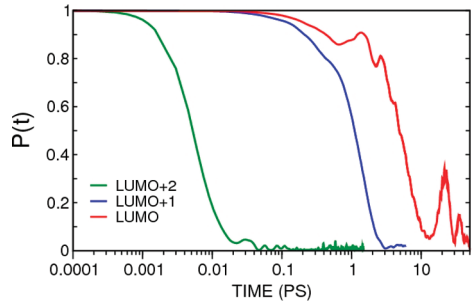

Figure 13. Survival probability for electron injection from the LUMO (red), LUMO+1 (blue), and LUMO+2 (green).

much slower (~50 ps) due to the smaller overlap of the electron donor and acceptor orbitals.

Figure 13 shows the evolution of the time-dependent electronic population $P(t)$ of photoexcited adsorbate complex **2**-TiO_2, shown in Figure 5. Here, interfacial electron injection from the LUMO and LUMO+1 is also complete in the 1−10 ps, while the injection from the benzo(f)quinoline LUMO+2 is much faster (10 fs), even faster than in the **1**-TiO_2 system.

The characteristic injection times reported in Figures 12 and 13 are mostly determined by the symmetry of the photoexcited electronic state, initially localized in the adsorbate molecule, and the extent of its overlap with the electronic states in the conduction band of the TiO_2 host substrate. When compared to the interfacial electron transfer from the LUMO+2, the injections from the LUMO and LUMO+1 are slower because these states are delocalized over the ligands Q(b) and Q(c), away from the TiO_2 surface. In contrast, injection from the LUMO+2 is ultrafast (complete within 10 fs) since it is localized in the Q(a) ring with significant coupling with the TiO_2 surface.

As extensively discussed in the literature, interfacial electron transfer (IET) in sensitized semiconductors is generally complete in <100 fs,[21] due to the strong coupling between the adsorbate and the substrate, a time scale much shorter than nuclear reorganization. Therefore, IET cannot be described by Marcus theory, which is based on the solvent reorganization and is valid only in the weak-coupling limit (e.g., for weakly coupled redox species separated by solvent). Thus, structural reorganization of the dye is not taken into account during the photoinjection calculations, since the structural reorganization should have little influence on the fastest injection dynamics of Figures 12 and 13. The reorganization of the geometry as well as the thermal nuclear fluctuations should, however, affect the slower injection dynamics. Previous studies indicate that the thermal fluctuations speed up the interfacial electron transfer dynamics by introducing additional relaxation pathways for electron transfer and diffusion.[11,28]

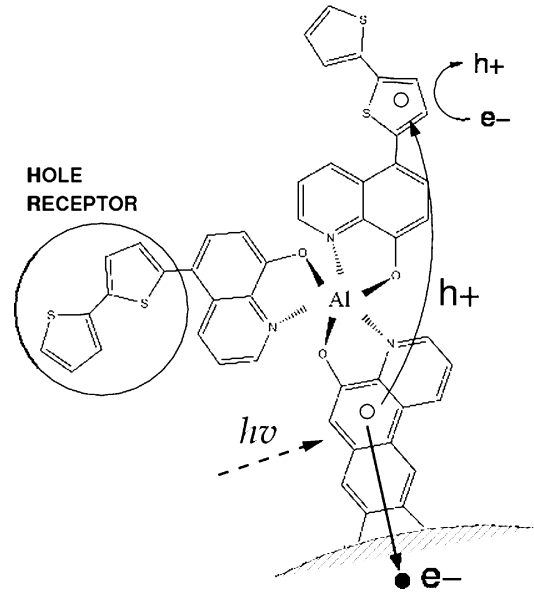

Figure 14. Charge transfer processes induced by photoexcitation of **2**-dithiophene/TiO_2.

5. Alq3-dithiophene/TiO_2

The results presented in previous sections predict visible light sensitization and ultrafast interfacial electron injection in TiO_2 surfaces when covalently functionalized with Alq3 adsorbates. An important advantage of Alq3, when compared to the classic Ru(II)-polypyridyl complexes of typical dye-sensitized solar cells, is that Alq3 is based on an inexpensive metal (Al). In addition, Alq3 is relatively small, therefore ideally suited to enhance surface coverage and photoabsorption efficiency. Furthermore, Alq3 can be functionalized with thiophene substituents to obtain efficient electron transport materials,[58,76−79] as found in poly(3-hexylthiophene) polymers most often used in Alq3 OLEDs. These oligothiophene polymers can lead to highly stable sensitizer assemblies for dye-sensitized solar cells.[23,80] Here, we analyze the derivatization of **2**-TiO_2 with dithiophene fragments substituting the phenoxide ring of the quinoline ligands (see Figure 14). The resulting molecular assembly exploits the optical properties of Alq3 and the hole transport functionality of oligothiophene polymers. A synthetic route for the production of 8-hydroxyquinoline derivatized with oligothiophenes can be obtained from recently published synthetic procedures.[81] We emphasize that our study is focused on TiO_2/Alq3-thiophene under low covarage, where there is no intermolecular charge transfer. Advantages of the molecular assembly, shown in Figure 14, are 2-fold: (1) the hole can relax into the oligothiophenes as soon as the electron is photoinjected into the TiO_2 surface, improving electron−hole separation and hindering recombination; (2) the oligothiophenes could bind I_3^- for rapid redox regeneration. Effective hole transport, however, requires a suitable order of energy levels. The occupied band of electronic states in the polymer must be above the HOMO of the Alq3 adsorbate to induce directionality of hole transport away from the functionalized surface. An excellent review of the physical chemistry mechanisms involved in the process of intramolecular electron−hole separation is provided by Brédas and coworkes.[22]

Figure 15a shows the total DOS of the **2**-dithiophene/TiO_2 nanostructure and the PDOS into the adsorbate **2** and dithiophene components. These results are consistent with the HOMO−LUMO gap (3.53 eV) of dithiophene determined by cyclic voltammetry measurements.[82] Figure 15a shows that the dithiophene moiety

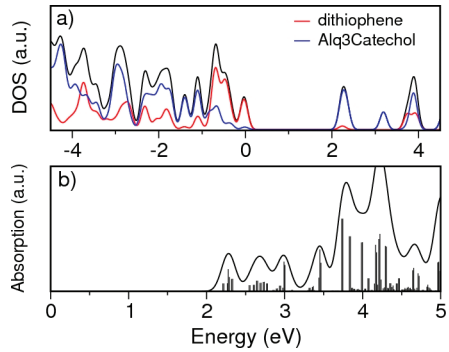

Figure 15. (a) Electronic density of states of the **2**-dithiophene/TiO_2 (black) and projected DOS into the dithiophene (red) and **2** (blue) moieties. (b) Photoabsorption spectrum of **2**-dithiophene/TiO_2, obtained according to the EH methodology.

introduces a band of occupied states just above the HOMO of Alq3, suggesting that photogenerated holes in Alq3 could spontaneously relax into the dithiophenes. In addition, it is shown that the HOMO−LUMO gap is very similar to the band gap in **2**-TiO_2, suggesting that thiophenes should not affect the optical properties Alq3 sensitizers. These results are consistent with the calculated photoabsorption spectrum of **2**-dithiophene/TiO_2, shown in Figure 15b.

6. Conclusions

We conclude that TiO_2 surfaces can be sensitized to visible light by functionalization with inexpensive Alq3 complexes commonly applied as optical medium components in highly efficient OLEDs. Alq3 complexes with hydroxylated benzoquinoline moieties produce robust molecular photosensitizers that bind to the TiO_2 by forming Ti−O covalent bonds. Upon visible light photoexcitation, the complexes promote ultrafast interfacial electron injection into the TiO_2 host substrate, leading to electron−hole separation through an operational mode that is reverse relative to the electron−hole pair recombination in OLED devices. We also conclude that the resulting Alq3 surface complexes could be derivatized with oligothiophenes to obtain stable sensitizer assemblies where electron−hole pair recombination is hindered by hole transport along the oligothiophene polymers. The reported results are therefore expected to motivate the development of Alq3 based dye-sensitized solar cells, building upon existing technology gained from the fabrication of solid-state Alq3 electroluminescent devices.

Acknowledgment. L.G.C.R. and R.S. acknowledge financial support from CNPq/Brazil and computer allocation time from CENAPAD/Campinas, Brazil. V.S.B. acknowledges a generous allocation of DOE supercomputer time from the National Energy Research Scientific Computing Center (NERSC) and financial support from the Grants NSF ECCS 0404191 and DOE DE-FG02-07ER15909.

Supporting Information Available: Ground-state geometries for computational models of complex **1**-TiO_2 and complex **2**-TiO_2. This material is available free of charge via the Internet at http://pubs.acs.org.

References and Notes

(1) Tang, C. W.; VanSlyke, S. A. *Appl. Phys. Lett.* **1987**, *51*, 913–915.
(2) *Organic Light Emitting Devices: Synthesis, Properties and Applications*; Müllen, K., Scherf, U., Eds.; Wiley-VCH: New York, 2006.
(3) Li, Z. R.; Meng H. *Organic Light-emitting Materials and Devices*; CRC Press: New York, 2007.
(4) Helfrich, W.; Schneidere, W. G. *Phys. Rev. Lett.* **1965**, *14*, 229–231.
(5) Dresner, J. *RCA Rev.* **1969**, *30*, 322.
(6) Tang, C. W.; VanSlyke, S. A.; Chen, C. H. *J. Appl. Phys.* **1989**, *65*, 3610–3616.
(7) Burrows, P. E.; Shen, Z.; Bulovic, V.; McCarty, D. M.; Forrest, S. R.; Cronin, J. A.; Thompson, M. E. *J. Appl. Phys.* **1996**, *79*, 7991–8006.
(8) VanSlyke, S. A.; Chen, C. H.; Tang, C. W. *Appl. Phys. Lett.* **1996**, *69*, 2160–2162.
(9) H. Aziz, H.; Popovic, Z. D.; Hu, N. X.; Hor, A. M.; Xu, G. *Science* **1999**, *283*, 1900–1902.
(10) Rego, L. G. C.; Batista, V. S. *J. Am. Chem. Soc.* **2003**, *125*, 7989–7997.
(11) Abuarbara, S. G.; Rego, L. G. C.; Batista, V. S. *J. Am. Chem. Soc.* **2005**, *127*, 18234–18242.
(12) Rego, L. G. C.; Abuabara, S. G.; Batista, V. S. *J. Chem. Phys.* **2005**, *122* (1−6), 154709.
(13) Abuabara, S. G.; Cady, C. W.; Baxter, J. B.; Schmuttenmaer, C. A.; Crabtree, R. H.; Brudvig, G. W.; Batista, V. S. *J. Phys. Chem. C* **2007**, *111*, 11982–11990.
(14) McNamara, W. R.; Snoeberger III, R. C.; Li, G.; Schleicher, J. M.; Cady, C. W.; Poyatos, M.; Schmuttenmaer, C. A.; Crabtree, R. W.; Brudvig, G. W.; Batista, V. S. *J. Am. Chem. Soc.* **2008**, *130*, 14329–14338.
(15) Kim, H. S.; Kim, C. H.; Ha, C. S.; Lee, J. K. *Synth. Met.* **2001**, *117*, 289–291.
(16) Vivo, P.; Jukola, J.; Ojala; Chukharev, V.; Lemmetyinen, H. *Sol. Energy Mater. Sol. Cells* **2008**, *92*, 1416–1420.
(17) Barra, M.; Cassinese, A.; D'Angelo, P.; Hueso, L. E.; Graziosi, P.; Dediu, V. *Org. Electr.* **2008**, *9*, 911–915.
(18) Ishii, H.; Yoshimura, D.; Sugiyama, K.; Narioka, S.; Hamatani, Y.; Kawamoto, I.; Miyazaki, T.; Ouchi, Y.; Seki, K. *Synth. Met.* **1997**, *85*, 1389–1390.
(19) Curioni, A.; Andreoni, W. *IBM J. Res. Dev.* **2001**, *45*, 101–113.
(20) Yanagisawa, S.; Morikawa, Y. *Chem. Phys. Lett.* **2006**, *420*, 523–528.
(21) (a) Shane, A.; Meyer, G. J. *Chem. Soc. Rev.* **2009**, *38*, 115–164. (b) Yum, J.-H.; Chen, P.; Grätzel, M.; Nazeeruddin, K. *ChemSusChem.* **2008**, *1*, 699–707. (c) Grätzel., M. *Inorg. Chem.* **2005**, *44*, 6841–6951.
(22) Bredas, J. L.; Beljonne, B.; Coropceanu, V.; Cornil, J. *Chem. Rev.* **2004**, *104*, 4971–5004.
(23) Hammann, T. W.; Jensen, R. A.; Martinson, A. B. F.; Ryswyk, H. V.; Hupp, J. T. *Energy Environ. Sci.* **2008**, *1*, 66–78.
(24) (a) O'Regan, B.; Grätzel., M. *Nature* **1991**, *353*, 737–740. (b) Grätzel., M. *Nature* **2001**, *414*, 338–344.
(25) Kuzetsov, A. M.; Ulstrup, J. *Electron transfer in chemistry and biology: An introduction to the theory*; Wiley-VCH: New York, 1999.
(26) May, V.; Kühn, O. *Charge and energy transfer dynamics in Molecular systems: A theoretical introduction*; Wiley-VCH: New York, 2000.
(27) Schatz, G. C.; Ratner, M. A. *Quantum Mechanics in Chemistry*; Dover: Mineola, NY, 2002.
(28) Duncan, W. R.; Prezhdo, O. V. *Annu. Rev. Phys. Chem.* **2007**, *58*, 143–184.
(29) (a) Becke, A. D. *J. Chem. Phys.* **1993**, *98*, 1372–1377. (b) Becke, A. D. *J. Chem. Phys* **1993**, *98*, 5648–5652.
(30) Frisch, M. J.; Trucks, G. W.; Schlegel, H. B.; Scuseria, G. E.; et al. *Gaussian 03*, revision C02; Gaussian, Inc.: Wallingford, CT, 2004.
(31) Kresse, G.; Furthmuller, J. *Vienna ab initio Simulation Package (VASP)*; University of Vienna: Vienna, Austria, 2001.
(32) Kresse, G.; Furthmuller, J. *Comput. Mater. Sci.* **1996**, *6*, 15–50.
(33) Hafner, J. *Comput. Phys. Commun.* **2007**, *177*, 6–13.
(34) Field, M. J. *A Practical Introduction to the Simulation of Molecular Systems*, 2nd ed.; Cambridge University Press: Cambridge, U.K., 2007.
(35) Hoffman, R. *Rev. Mod. Phys.* **1988**, *60*, 601–628.
(36) Burdett, J. K. *Chemical Bonding in Solids*; Oxford University Press: Oxford, 1995.
(37) Cerdá, J. S. *Phys. Rev. B* **2000**, *61*, 7965–7971.
(38) Kirczenow, G. *The Oxford Handbook of Nanoscience and Technology: Volume I*; Narlikar, A. V., Fu, Y. Y., Eds.; Oxford University Press: Oxford, 2009.
(39) McGlynn, S. P.; Vanquickenborne, L. G.; Kinoshita, M.; Carroll, D. G. *Introduction to Applied Quantum Chemistry*; Holt, Rinehart and Winston INC.: New York, 1972.
(40) Ammeter, J. H.; Buergi, H. B.; Thibeault, J. C.; Hoffmann, R. *J. Am. Chem. Soc.* **1978**, *100*, 3686–3692.
(41) Table of parameters for Extended Hückel Calculations, collected by Santiago Alvarez, Universitat de Barcelona (1995).
(42) Huber, R.; Moser, J. E.; Grätzel, M.; Wachtveitl, J. *J. Phys. Chem. B* **2002**, *106*, 6494–6499.
(43) (a) Gundlach, L.; Ernstorfer, R.; Willig, F. *Phys. Rev. B* **2006**, *74* (1−10), 035324. (b) Ernstorfer, R.; Gundlach, L.; Felber, S.; Storck, W.;

Eichberger, R.; Willig, F. *J. Phys. Chem. B* **2006**, *110*, 25383–25391. (c) Gundlach, L.; Ernstorfer, R.; Willig, F. *Prog. Surf. Sc.* **2007**, *82*, 355–377.
(44) Stier, W.; Duncan, W. R.; Prezhdo, O. V. *Adv. Mater.* **2004**, *16*, 240–244.
(45) Duncan, W. R.; Stier, W. M.; Prezhdo, O. V. *J. Am. Chem. Soc.* **2005**, *127*, 7941–7951.
(46) Kondov, I.; Cizek, M.; Benesch, C.; Wang, H.; Thoss, M. *J. Phys. Chem. C* **2007**, *111*, 11970–11981.
(47) Meng, S.; Ren, J.; Kaxiras, E. *Nano Lett.* **2008**, *8*, 3266–3272.
(48) Calzaferri, G.; Rytz, R. *J. Phys. Chem.* **1995**, *99*, 12141–12150.
(49) Ema, I.; López, R.; Fernández, J. J.; Ramírez, G.; Rico, J. F. *Int. J. Quantum Chem.* **2008**, *108*, 25–39.
(50) Wang, L.; Willig, F.; May, V. *J. Chem. Phys.* **2007**, *126* (1−12), 134110.
(51) Amati, M.; Lelj, F. *J. Phys. Chem. A* **2003**, *107*, 2560–2569.
(52) Halls, M. D.; Schlegel, H. B. *Chem. Mater.* **2001**, *13*, 2632–2640.
(53) Hopkins, T. A.; Meerholz, K.; Shaheen, S.; Anderson, M. L.; Schmidt, A.; Kippelen, B.; Padias, A. B.; Hall, H. K.; Peyghambarian, N.; Armstrong, N. R. *Chem. Mater.* **1996**, *8*, 344–351.
(54) (a) Curioni, A.; Boero, M.; Andreoni, W. *Chem. Phys. Lett.* **1998**, *294*, 263–271. (b) Curioni, A.; Boero, M.; Andreoni, W. *J. Am. Chem. Soc.* **1999**, *121*, 8216–8220.
(55) Ravi Kishore, V. V. N.; Aziz, A.; Narasimham, K. L.; Periasamy, N.; Meenakshi, P. S.; Wategaonkar, S. *Synth. Met.* **2002**, *126*, 199–205.
(56) Huber, R.; Spörlein, S.; Moser, J. E.; Grätzel, M.; Wachtveitl, J. *J. Chem. Phys. B* **2000**, *104*, 8995–9003.
(57) Duncan, W. R.; Prezhdo, O. V. *J. Phys. Chem. B* **2005**, *109*, 365–373.
(58) Meyers, A.; Weck, M. *Chem. Mater.* **2004**, *16*, 1183–1188.
(59) VanSlyke, S. A.; Bryan, P. S.; Lovecchio, F. V. Blue emitting internal junction organic electroluminescent device (II). U.S. Patent 5,150,006, September 22, 1992.
(60) Garbuzov, D. Z.; Bulović, V.; Burrows, P. E.; Forrest, S. R. *Chem. Phys. Lett.* **1996**, *249*, 433–437.
(61) Brinkmann, M.; Gadret, G.; Muccini, M.; Taliani, C.; Masciocchi, N.; Sironi, A. *J. Am. Chem. Soc.* **2000**, *122*, 5147–5157.
(62) Freeman, D. C., Jr.; White, C. E. *J. Am. Chem. Soc.* **1956**, *78*, 2678–2682.
(63) Choy, W. C. H.; Fong, H. H. *J. Phys. D: Appl. Phys.* **2008**, *41* (1−7), 155109.
(64) Ogawa, N.; Miyata, A.; Tamaru, H.; Suzuki, T.; Shimada, T.; Hasegawa, T.; Saiki, K.; Miyano, K. *Chem. Phys. Lett.* **2008**, *450*, 335–339.
(65) Klevens, H. B.; Platt, J. R. *J. Chem. Phys.* **1949**, *17*, 470–481.
(66) Rice, C. R.; Ward, M. D.; Nazeeruddin, M. K.; Grätzel, M. *New. J. Chem.* **2000**, *24*, 651–652.
(67) Verma, S.; Kar, P.; Das, A.; Palit, D. K.; Ghosh, H. N. *J. Chem. Phys. C* **2008**, *112*, 2918–2926.
(68) Redfern, P. C.; Zapol, P.; Curtiss, L. A.; Rajh, T.; Thurnauer, M. C. *J. Phys. Chem. B* **2003**, *107*, 11419–11427.
(69) Xu, Y.; Chen, W. K.; Liu, S. H.; Cao, M. J.; Li, J. Q. *Chem. Phys.* **2007**, *331*, 275–282.
(70) Addy, P.; Evans, D. F.; Sheppard, R. N. *Inorg. Chim. Acta* **1987**, *127*, L19–L20.
(71) Kushto, G. P.; Iizumi, Y.; Kido, J.; Kafafi, Z. H. *J. Phys. Chem. A* **2000**, *104*, 3670–3680.
(72) Wang, Y.; Hang, K.; Anderson, N. A.; Lian, T. *J. Chem. Phys. B* **2003**, *107*, 9434–9440.
(73) Rodriguez, R.; Blesa, M. A.; Regazzoni, A. E. *J. Colloid Interface Sci.* **1996**, *177*, 122–131.
(74) Liu, Y.; Dadap, J. I.; Zimdars; Eisenthal, K. B. *J. Phys. Chem B* **1999**, *103*, 2480–2486.
(75) Persson, P.; Bergstrom, R.; Lunell, S. *J. Phys. Chem. B* **2000**, *104*, 10348–10351.
(76) Meyers, A.; Weck, M. *Macromolecules* **2003**, *36*, 1766–1768.
(77) Snaith, H. J.; Schmidt-Mende, L. *Adv. Mater.* **2007**, *19*, 3187–3200.
(78) Nespurek, T.; Toman, P.; Mensik, M.; Kratochvilova, I.; Sworakowski, J.; Mallouk, T. E. *J. Optoelectronics Adv. Mater.* **2007**, *9*, 134–140.
(79) Rodriguez, F.; Yassar, A.; Fave, J. L.; Roussel, J.; Maurel, F.; Horowitz, G. *Proc. SPIE* **2006**, *6192*, 619238.
(80) Katoh, R.; Akihiro, F.; Shogo, M.; Miyashita, M.; Sunahara, K.; Koumura, N.; Hara, K. *Energy Environ. Sci.* **2009**, *2*, 542–546.
(81) Wang, Z. S.; Koumura, N.; Cui, Y.; Takahashi, M.; Sekiguchi, H.; Mori, A.; Kubo, T.; Furube, A.; Hara, K. *Chem. Mater.* **2008**, *20*, 3993–4003, including the Supporting Information.
(82) Hsu, C. W.; Wang, L.; Su, W. F. *J. Colloid Interface Sci.* **2009**, *329*, 182–187.

JP9094479